The Journal of Navigation (2021), **74**:5 1057–1072
doi:10.1017/S0373463321000308

CAMBRIDGE UNIVERSITY PRESS

RESEARCH ARTICLE

A bionic point-source polarisation sensor applied to underwater orientation

Teng Zhang,[1] Jian Yang,[1,2,3]* Lei Guo,[1,2,3] Pengwei Hu,[1] Xin Liu,[1] Panpan Huang,[3] and Chenliang Wang[1,2,4]

[1] School of Automation Science and Electrical Engineering, Beihang University, Beijing, China.
[2] Beijing Advanced Innovation Centre for Big Data-Based Precision Medicine, School of Medicine and Engineering, Beihang University, Beijing, China.
[3] Hangzhou Innovation Institute, Beihang University, Hangzhou, China.
[4] Key Laboratory of Big Data-Based Precision Medicine, Ministry of Industry and Information Technology, Beihang University, Beijing, China.
*Corresponding author. E-mail: jyang_buaa@buaa.edu.cn

Received: 10 June 2020; **Accepted:** 6 March 2021; **First published online:** 4 May 2021

Keywords: sensor, modelling, animal navigation, underwater navigation

Abstract

With the characteristics of full autonomy and no accumulated errors, polarisation navigation shows tremendous prospects in underwater scenarios. In this paper, inspired by the polarisation vision of aquatic organisms, a novel point-source polarisation sensor with high spectral adaptability (400 nm–760 nm) is designed for underwater orientation. To enhance the environmental applicability of the underwater polarisation sensor, a novel sensor model based on the underwater light intensity attenuation coefficient and optical coupling coefficient is established. In addition, concerned with the influence of light intensity uncertainty on sensor performance underwater, an antagonistic polarisation algorithm is adopted for the first time, to improve the accuracy of angle of polarisation and degree of polarisation in the low signal-to-noise ratio environment underwater. Finally, indoor and outdoor experiments are carried out to evaluate the performance of the designed polarisation sensor. The results show that the designed point-source polarisation sensor can acquire polarised light and be used for heading determination underwater.

1. Introduction

Autonomous underwater vehicles (AUVs) play an important role in marine environment modelling, underwater target recognition, geological surveys, etc. (Miller et al., 2010; Ma et al., 2019). One of the challenges to realise an AUV is to obtain precise attitude information. There have been many methods proposed for attitude estimation. For example, the global navigation satellite system (GNSS) carrier phase-based method with ambiguity resolution is proposed to determine a vehicle's attitude (Giorgi et al., 2010). Nevertheless, this method cannot be used for AUVs as it is difficult to receive the satellite signals due to the rapid decay of radio signals underwater (Paull et al., 2014; Emami and Taban, 2018). Another commonly used method of attitude determination is based on the inertial navigation system (INS) (Caruso, 2000; Xian et al., 2015). However, the attitude error obtained by the INS accumulates over time (Stutters et al., 2008; Wang et al., 2016). To overcome the problem of error accumulation, Huang et al. (2015) proposed a type of full attitude determination approach based on the Earth's magnetic gradient tensor measurement, and proved the attitude determination algorithm. However, geomagnetic measurements are susceptible to disturbances caused by the uncertain magnetic

field underwater (Wu et al., 2018). To endow the AUV with intelligent sensing capability and intelligent behaviour, one key technology is to realise autonomous navigation and localisation without external transmission and information exchange (Huang et al., 2019).

It has been illustrated that the atmospheric polarisation pattern can be acquired for orientation by insects, such as desert ants and honey bees. They can navigate by sensing the polarised light during foraging, migrating and homing (Müller and Wehner, 1988; Heinze and Homberg, 2007). Currently, there are two types of polarisation sensors used to measure polarised light: point-source based and image-based sensors. Lambrinos designed a bionic polarisation compass with photosensitive diodes and successfully fitted it on a robot for navigation (Lambrinos et al., 1997). Another study focused on the orientation algorithm with bionic polarisation compass and an integrated navigation method based on the optical compass and multi-sensors (Wang et al., 2017), then developed point-source-based and camera-based polarisation sensors for navigation in the atmosphere (Xian et al., 2014; Fan et al., 2016). Chahl and Mizutani (2012) developed two biomimetic polarisation sensors that use the spectral, spatial and skylight polarisation pattern for navigation and stabilisation, and conducted flight tests using the biomimetic sensors for maintaining level flight, which is promising for use in miniaturising the autopilots of small unmanned aerial vehicles. Dupeyroux et al. designed a six-legged walking robot equipped with two ultraviolet light polarisation sensors and demonstrated the effectiveness of polarised light navigation with experiments without using GNSS (Dupeyroux et al., 2017, 2019a, 2019b). Yang et al. (2019) proposed a polarisation attitude and heading reference system to address the autonomous attitude and heading determination challenge in GNSS-denied and magnetic disturbed scenarios. Subsequently, they presented a self-positioning system using polarisation pattern for the location of users (Yang et al., 2020).

Interestingly, it has been found that aquatic organisms can also gain navigation information by sensing the polarised light underwater with their special visual systems (Thoen et al., 2014). There are two types of underwater polarisation patterns based on Snell's window (Waterman, 1954). One pattern, similar to the atmospheric polarisation pattern (Sabbah et al., 2006), is in the refraction window, which relies on single Rayleigh scattering of the corresponding medium underwater (Waterman, 2006). The other pattern, produced by the interaction between water and sunlight entering the water, is out of the refraction window, which is ubiquitous and perpendicular to the direction of underwater light. In the past decade, the underwater polarisation pattern has been widely studied. Sabbah and colleagues studied the underwater light polarisation near sunrise and the possibility of using underwater polarisation light for navigation under restricted conditions (Sabbah and Shashar, 2007; Lerner et al., 2011). Zhou et al. (2017) took the wind speed disturbance into consideration and proposed a model of the underwater polarisation pattern with refracted sky lights when the water surface fluctuates. Cheng et al. (2019) proposed a numerical model based on Stokes vector and Mueller matrix to simulate the underwater polarisation distribution by considering the atmospheric polarisation pattern, water–air interface refraction and single Rayleigh scattering of water molecules.

Underwater biomimetic polarisation has attracted extensive attention from scholars all over the world. There have been a few underwater polarisation sensors developed to gain insight into heading determination and positioning with the underwater polarised light. Powell et al. (2018) used a bioinspired polarisation-sensitive imager to determine the geographic location of the observer based on the underwater polarisation pattern. They used two underwater polarisation video cameras to acquire polarised light. A waterproof single-pixel version of the polarisation compass was developed, which was successfully tested underwater in 2019 (Dupeyroux et al., 2019b). It consists of an ultraviolet (UV)-sensitive photodiode and a linear polariser. The spectral sensitivity of this compass ranged from 200 to 375 nm. In addition, they proposed a strategy to acquire accurate measurements for the heading angle by combining the scanning and simultaneous modes into a UV-polarised light scanning model. However, the large size of an underwater polarisation video camera makes it difficult to install on AUVs. It has also been suggested that polarised light in water differs from that in air, and that marine invertebrates tend to be maximally sensitive to wavelength near 500 nm underwater (Cronin and Shashar, 2001). In addition, due to the optical coupling effects of reflection, refraction and scattering underwater, the polarised light

https://doi.org/10.1017/S0373463321000308 Published online by Cambridge University Press

intensity shows high uncertainty. As a result, the existing polarisation sensor accuracy degrades in the low signal-to-noise ratio (SNR) environment underwater.

In this paper, inspired by the polarisation sensitivity mechanism of the mantis shrimp, a bionic point-source underwater polarisation sensor is developed. The main technical features in this paper are briefly summarised as follows:

1. Inspired by the mid-band region polarisation perception opposite structure of the mantis shrimp, a bionic point-source underwater polarisation sensor is designed. To simulate the polarisation receptor of marine animals with spectral sensitivity near 500 nm, the designed sensor is capable of measuring the light at wavelengths of 400 and 760 nm. In this way, the spectral adaptability of the underwater polarisation sensors can be increased.
2. The influence of the depth and turbidity of water on the sensor performance is analysed quantitatively, and a novel underwater polarisation sensor model based on light intensity attenuation coefficient is established. The coupling effects of the stray light caused by the adjacent channels are specially considered in the sensor modelling. In addition, the antagonistic polarisation algorithm is adopted to calculate angle of polarisation (AoP) and degree of polarisation (DoP) with high accuracy. The interference of light intensity inconsistency underwater can then be reduced. As such, the accuracy of AoP and DoP can be improved in the low SNR underwater environment.

The remainder of this paper is arranged as follows. In Section 2, the design of the polarisation sensor with respect to its principle and hardware is introduced; In Section 3, the effects of depth, turbidity and optical coupling underwater on sensor performance are taken into consideration, and a novel sensor model based on the underwater light intensity attenuation coefficient and optical coupling coefficient is then presented. In Section 4, an antagonistic polarisation algorithm is introduced for the first time for use in the low SNR environment underwater. In Section 5, the least squares method to identify the sensor parameters is described. To evaluate the performance of the designed polarisation sensor, both indoor and outdoor underwater experiment results and analyses are presented in Section 6, and Section 7 presents the conclusions.

2. Underwater polarisation sensor design

There is a mid-band region at the back of the compound eye of the mantis shrimp, which is between the dorsal peripheral region and ventral peripheral region, as shown in Figure 1 (Thoen et al., 2014, 2017). This region specialises in colour and polarisation vision, which consists of six ommatidial rows. The fifth and sixth rows of the mid-band region can perceive linear polarised light and circularly polarised light. The arrangement direction of microvilli in the photosensitive fine is the vertical state between parallel groups, forming a photosensitive channel that can perceive a pair of orthogonal linear polarised lights (Kleinlogel et al., 2003; Kleinlogel and Marshall, 2006). In this way, the signals obtained by the photosensitiser will form an antagonistic effect, which can improve the intensity and contrast of a polarisation signal (How et al., 2014).

Simulating the polarisation perception structure and signal processing mechanism of the mantis shrimp, an underwater bionic polarisation sensor is developed based on photoelectric detection. Compared with the ultraviolet-sensitive polarisation sensor, it can trap visible light at wavelengths between 400 and 760 nm so that the sensor's spectral adaptability is improved underwater. The designed sensor consists of three groups of perpendicular polarisation detection channels, the polarisation detection directions of which are 0° and 90°, 30° and 120°, 60° and 150°, respectively, as shown in Figure 2.

The whole sensor adopts a circular design for miniaturisation. There is a protective device on the top of the sensor, composed of a protective cover, a sensor ferrule and a transmittance glass, to protect the polariser below and block the stray light around the sensor. To prevent light leakage between each channel, a light leakage prevention device is added. In addition, a square groove is provided at the light intensity input window, which is convenient to control the polarisation detection direction of different channels. On the basis of a large number of experimental trials, a light intensity input window

https://doi.org/10.1017/S0373463321000308 Published online by Cambridge University Press

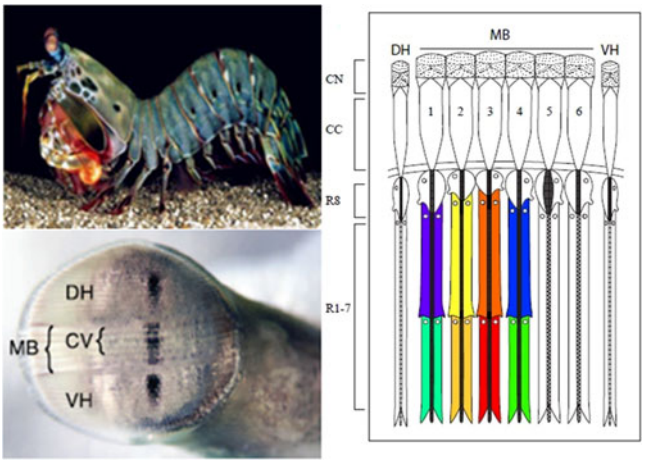

Figure 1. *Polarisation sensing structure of the mantis shrimp.*

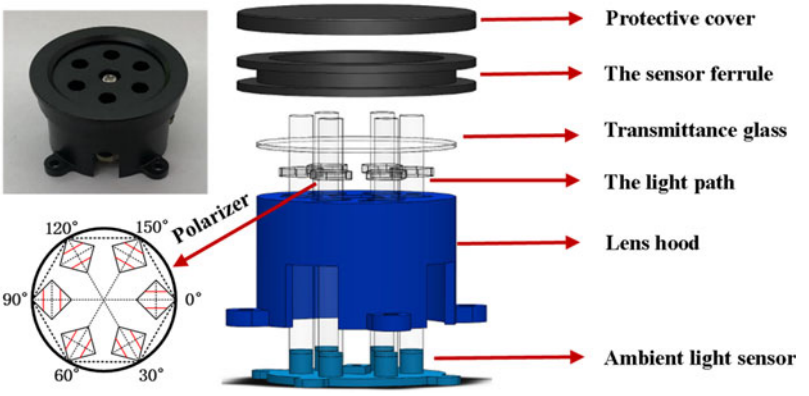

Figure 2. *Schematic diagram of underwater polarisation sensor design.*

with a radius of just 1·5 mm is set up to achieve polarised light spot observation as much as possible underwater, and a photosensitive chip is installed at the bottom of the window. The diameter and height of the designed sensor are 25 mm and 18 mm, respectively.

The BH1750FVI photosensitive chip is used as the photoreceptor. Its features are shown in Table 1. It is a 16-bit digital ambient light sensor integrated circuit that can detect a wide range of light (1 lx–65535 lx) at high resolution. As this sensor does not depend on the light source and can resist the influence of infrared, the partial spectrum influence underwater can be avoided. To ensure the consistency of the input light, the photosensitive chip is placed as close as possible to the optical path input window. In addition, the whole sensor is designed with black non-reflective material to absorb the oblique light of the sensor inner surface and the scattered light partially reflected by the sensor outer surface underwater. As a result, the interference of external stray light on the optical path can be reduced.

The underwater bionic polarisation sensor receives the light signals of each channel from the dot-circle input window. The AoP and DoP can then be calculated in real time. The light intensity and polarisation information can also be shared in real time. The designed polarisation sensor features low power consumption, compact size and high real-time capability. The power consumption of sensor is 0·003 W, the height is 18 mm and the diameter is 25 mm.To realise underwater autonomous navigation for different kinds of underwater vehicles, the sensor can be combined with other navigation systems, such as INS, acoustic navigation, etc.

https://doi.org/10.1017/S0373463321000308 Published online by Cambridge University Press

Table 1. *The features of the main sensor elements.*

Main elements	Features
Transmittance glass	Effective transmission: 97·5%–99·7% Transmitted wavelength: 400 nm–760 nm
Polariser	Size: 4 mm × 4 mm × 0·18 mm Spectral range: 400 nm–760 nm
Polariser	Extinction ratio: 9000:1
Ambient light sensor (BH1750FVI)	Wide measurement range: 1–65535 lx Max resolution: 0·5 lx
Polarisation sensor size	Diameter: 25 mm Height: 18 mm

3. Underwater sensor modelling

The polarised light can be influenced by many indeterminacy factors underwater, such as reflection, refraction, the scattering of water, etc. In particular, the depth and turbidity of the water will bring greater uncertainty to the underwater polarised light intensity. In addition, in each detection channel of the sensor, the stray light caused by adjacent channels can also bring uncertainty to the light intensity of the sensor, especially in the low SNR underwater environment. As such, the existing polarisation sensor model is inapplicable underwater. Addressing this issue, the effect of multi-source interference on the performance of the polarisation sensor is analysed, and the underwater polarisation sensor model based on light intensity attenuation coefficient and optical coupling coefficient is established in this section.

In the air conditions, the polarisation sensor model (Lambrinos et al., 1997) is generally expressed as:

$$f(d,\phi) = \sigma_{\text{in}} I_{\text{in}}(1 + d\cos 2(\phi + \alpha)) \tag{1}$$

where $f(d,\phi)$ is the output light intensity; I_{in} is the input light intensity; d and ϕ are DoP and AoP, respectively; α is the installation angle of the polariser; and σ_{in} is the light intensity coefficient representing the gain and loss of the light intensity of the whole sensor channel.

In comparison with the air conditions, the underwater light intensity will damp rapidly with the increase of the depth and turbidity of water. As such, to use polarised light for navigation, an underwater polarisation sensor model should be established. In general, the light intensity in water decays exponentially and can be expressed as (Kirk, 1983):

$$I_{\text{in}} = I_0 \mathrm{e}^{-kz} \tag{2}$$

where I_0 is the initial light intensity on the water, k is the underwater light intensity attenuation coefficient and z is the depth of water.

By substituting Equation (2) into Equation (1), the underwater polarised light intensity relevant to the depth and turbidity of water can be illustrated as follows.

$$f(d_w,\phi_w) = \sigma_{in} I_0 e^{-kz}(1 + d_w\cos 2(\phi_w + \alpha)) \tag{3}$$

In addition to the uncertainty of external ambient light, the sensor performance can be severely affected by the light pollution caused by itself. Ideally, the photoreceptor of each detection channel can only sense the polarised light intensity of the corresponding channel. However, due to limitations of manufacture technology, every detection channel will inevitably suffer from problems of light leakage. When the sensor is working, optical path coupling effects will occur between adjacent detection channels, as shown in Figure 3.

https://doi.org/10.1017/S0373463321000308 Published online by Cambridge University Press

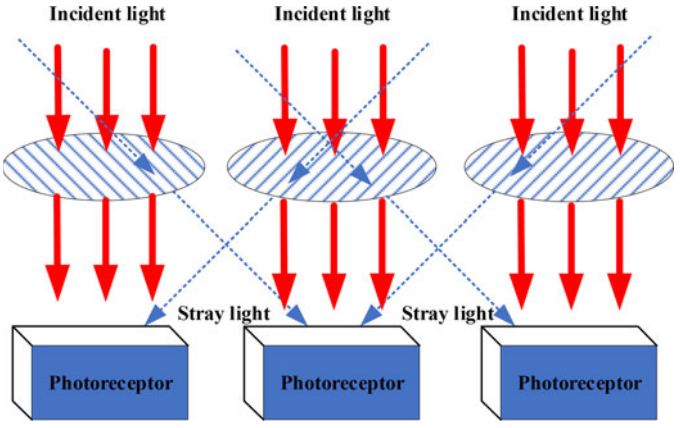

Figure 3. *Optical coupling effects.*

It is assumed that the output light intensities of two adjacent channels are $f_1(d_w, \phi_w)$ and $f_2(d_w, \phi_w)$, respectively. The stray polarised light intensities coupled to the detection channel can be expressed as:

$$\begin{aligned} f_{dis}^1(d_w, \phi_w) &= k_1 f_1(d_w, \phi_w) = k_1 \sigma_{in}^1 I_0 \mathrm{e}^{-\mathrm{kz}}(1 + d_w \cos 2(\phi_w + (\alpha - \pi/6)) \\ f_{dis}^2(d_w, \phi_w) &= k_2 f_2(d_w, \phi_w) = k_2 \sigma_{in}^2 I_0 \mathrm{e}^{-\mathrm{kz}}(1 + d_w \cos 2(\phi_w + (\alpha + \pi/6)) \end{aligned} \tag{4}$$

where the light intensity transfer coefficients of two adjacent channels are k_1 and k_2, respectively. Let $\sigma_1 = k_1 \sigma_{\mathrm{in}}^1$ and $\sigma_2 = k_2 \sigma_{\mathrm{in}}^2$, and Equation (4) can be transformed into

$$\begin{aligned} f_{\mathrm{dis}}^1(d_w, \phi_w) &= \sigma_1 I_0 e^{-kz}(1 + d_w \cos 2(\phi_w + (\alpha - \pi/6)) \\ f_{\mathrm{dis}}^2(d_w, \phi_w) &= \sigma_2 I_0 e^{-kz}(1 + d_w \cos 2(\phi_w + (\alpha + \pi/6)) \end{aligned} \tag{5}$$

According to the principle of scalar addition, the output light intensity of the detection channel with stray polarised light can be written as:

$$F(d_w, \phi_w) = f(d_w, \phi_w) + f_{\mathrm{dis}}^1(d_w, \phi_w) + f_{\mathrm{dis}}^2(d_w, \phi_w) \tag{6}$$

Expanding the formula, we get

$$\begin{aligned} F(d_w, \phi_w) = I_0 \mathrm{e}^{-kz} d_w [&(\sigma_{\mathrm{in}} + \sigma_1/2 + \sigma_2/2) \cos 2(\phi_w + \alpha) \\ &+ \sqrt{3}/2(\sigma_2 - \sigma_1) \sin 2(\phi_w + \alpha)] + I_0 \mathrm{e}^{-kz}(\sigma_{\mathrm{in}} + \sigma_1 + \sigma_2) \end{aligned} \tag{7}$$

Let

$$\begin{aligned} G_1 = \sigma_{\mathrm{in}} + (\sigma_1 + \sigma_2)/2, G_2 = \sqrt{3}/2(\sigma_2 - \sigma_1) \\ \cos\beta = G_1^2/\sqrt{G_1^2 + G_2^2}, \sin\beta = G_2^2/\sqrt{G_1^2 + G_2^2} \end{aligned} \tag{8}$$

In combination with Equation (7), Equation (5) can be written as:

$$F(d_w, \phi_w) = I_0 \mathrm{e}^{-kz} d_w \sqrt{G_1^2 + G_2^2} \cos 2(\phi_w + \alpha + \beta/2) + I_0 \mathrm{e}^{-kz}(\sigma_{in} + \sigma_1 + \sigma_2) \tag{9}$$

And then we set

$$\sqrt{G_1^2 + G_2^2} = \overline{\sigma}_I, (\sigma_{\mathrm{in}} + \sigma_1 + \sigma_2) = \overline{\sigma}_d, \alpha + \beta/2 = \psi \tag{10}$$

https://doi.org/10.1017/S0373463321000308 Published online by Cambridge University Press

Equation (10) can then be transformed into:

$$F(d_w, \phi_w) = I_0 e^{-kz} d_w \overline{\sigma}_I \cos 2(\phi_w + \psi) + I_0 e^{-kz} \overline{\sigma}_d \tag{11}$$

Let $\overline{\sigma}_I = \sigma_I, \overline{\sigma}_d / \overline{\sigma}_I = \sigma_d$, the sensor model can be presented in the following form

$$F(d_w, \phi_w) = \sigma_I I_0 e^{-kz} (1 + \sigma_d d_w \cos 2(\phi_w + \psi)) \tag{12}$$

where σ_I, σ_d and ψ are the light intensity coefficient, optical coupling coefficient and installation angle of the polariser.

Distinct from the existing models, Equation (12) takes into account the influence of polarised light intensity uncertainty caused by the depth and turbidity of water, and the stray polarised light brought up by the adjacent channels. The validity of the underwater polarisation model is demonstrated in the indoor calibration experiment in Section 6.

4. Underwater antagonistic polarisation algorithm

In the literature, the polarisation calculation method based on independent channel is employed to calculate the AoP and DoP. In this method, the AoP and DoP can be determined by selecting the measurements of any three of the six detection channels and shows high flexibility characteristics. However, the anti-interference ability to light intensity disturbance performs poorly and is inapplicable in underwater conditions. In this section, to enhance the environmental suitability of the underwater polarisation sensor, an antagonistic polarisation algorithm is presented. Suppose that the sensor measurement error is ignored, the polarisation resolution can be expressed as follows:

$$\frac{F_i(d_w, \phi_w)}{F_j(d_w, \phi_w)} = \frac{\sigma_{I_i} I_0 e^{-kz} (1 + \sigma_{d_i} d_w \cos 2(\phi_w + \psi_i))}{\sigma_{I_j} I_0 e^{-kz} (1 + \sigma_{d_j} d_w \cos 2(\phi_w + \psi_j))} \tag{13}$$

where $i = 1, 2, 3$ are three adjacent sensor channels, and $j = 4, 5, 6$ indicate the corresponding opposite channels. To calculate the polarisation information, we have

$$F_{ij} = \sigma_{ij} \frac{1 + \sigma_{d_i} d_w \cos 2(\phi_w + \psi_i)}{1 + \sigma_{d_j} d_w \cos 2(\phi_w + \psi_j)} \tag{14}$$

By eliminating the denominator and expanding, Equation (13) can be expressed as

$$\sigma_{ij} - F_{ij} = F_{ij} \sigma_{d_j} d_w \cos 2(\phi_w + \psi_j) - \sigma_{ij} \sigma_{d_i} d_w \cos 2(\phi_w + \psi_i) \tag{15}$$

The equation can be written as in the matrix form

$$\mathbf{L} = \boldsymbol{\lambda} \mathbf{X} \tag{16}$$

And we can transform Equation (14) into

$$[\sigma_{ij} - F_{ij}]_{3\times 1} = \begin{bmatrix} F_{ij}\sigma_{d_j} \cos 2\psi_j - \sigma_{ij}\sigma_{d_i} \cos 2\psi_i \\ \sigma_{ij}\sigma_{d_i} \sin 2\psi_i - F_{ij}\sigma_{d_j} \sin 2\psi_j \end{bmatrix}^T_{3\times 2} \begin{bmatrix} d_w \cos 2\phi_w \\ d_w \sin 2\phi_w \end{bmatrix}^T_{2\times 1} \tag{17}$$

The estimated value of $\mathbf{X}$ can be calculated with the least squares method

$$\hat{\mathbf{X}} = (\boldsymbol{\lambda}^{\mathbf{T}} \boldsymbol{\lambda})^{-1} \boldsymbol{\lambda}^{\mathbf{T}} \mathbf{L} \tag{18}$$

https://doi.org/10.1017/S0373463321000308 Published online by Cambridge University Press

Once $\hat{\mathbf{X}}$ is obtained, the AoP and DoP can be solved by

$$\begin{aligned}\widehat{\phi}_w &= 0.5 \arctan\left(\hat{\mathbf{X}}(2)/\hat{\mathbf{X}}(1)\right)\\ \hat{d}_w &= \sqrt{\hat{\mathbf{X}}(1)^2 + \hat{\mathbf{X}}(2)^2}\end{aligned} \tag{19}$$

where $\hat{\mathbf{X}}(1)$ and $\hat{\mathbf{X}}(2)$ are the estimated values of $\mathbf{X}(1)$ and $\mathbf{X}(2)$, respectively.

Compared with the independent polarisation algorithm based on independent channel, the antagonistic polarisation algorithm groups two measurement equations of opposite channel into one measurement equation, which can reduce the interference caused by the inconsistent light intensity of different channels. As such, the accuracy of AoP and DoP can be improved in the low SNR environment underwater. The indoor underwater experiment presented in Section 6.2 was conducted to prove the effectiveness of the antagonistic polarisation algorithm in different underwater environments.

5. Sensor calibration

In this section, the calibration algorithm to determine the unknown parameters in the sensor model is designed. Assuming that the initial AoP is ϕ_0 and the number of sampling is N, the AoP of nth sampling with the uniform sampling technique is $\phi_{w_n} = \phi_0 + 2\pi n/N$, $n = 0, 1, \ldots, N-1$. Without considering the measurement error, the output light intensity of ith channels is presented as:

$$F_i(d_{w_n}, \phi_{w_n}) = \sigma_{I_i} I_{in}(1 + \sigma_{d_i} d_{w_n} \cos 2\phi_{w_n} \cos 2\psi_i - \sigma_{d_i} d_{w_n} \sin 2\phi_{w_n} \sin 2\psi_i) \tag{20}$$

where $i = 1, \cdots, 6$. Subsequently, the light intensity of the sensor can be presented as

$$F_i(d_{w_n}, \phi_{w_n}) = \sigma_{I_i} I_{in}(1 + \sigma_{d_i} d_{w_n} \cos 2\phi_{w_n} \cos 2\psi_i - \sigma_{d_i} d_{w_n} \sin 2\phi_{w_n} \sin 2\psi_i) \tag{21}$$

we have

$$\mathbf{F}(d_{w_n}, \phi_{w_n}) = \begin{bmatrix} I_0 e^{-kz} \\ I_0 e^{-kz} d_w \cos 2\phi_{w_n} \\ d_{w_n} \sin 2\phi_{w_n} \end{bmatrix}^T_{N\times 3} \begin{bmatrix} \sigma_{I_i} \\ \sigma_{I_i}\sigma_{d_i} \cos 2\psi_i \\ -\sigma_{I_i}\sigma_{d_i} \sin 2\psi_i \end{bmatrix}^T_{3\times 6} \tag{22}$$

Then the estimated value $\hat{\mathbf{X}}$ can be calculated with the least squares algorithm, and the parameters can be calculated with the components of the $\hat{\mathbf{X}}$ matrix:

$$\begin{aligned}\sigma_{I_i} &= \hat{\mathbf{X}}(1, i)\\ \sigma_{d_i} &= \sqrt{\hat{\mathbf{X}}(2, i) \times \hat{\mathbf{X}}(2, i) + \hat{\mathbf{X}}(3, i) \times \hat{\mathbf{X}}(3, i)}/\hat{\mathbf{X}}(1, i)\\ \psi_i &= 0.5 \arctan\left(\hat{\mathbf{X}}(2, i)/-\hat{\mathbf{X}}(3, i)\right)\end{aligned} \tag{23}$$

To prevent the estimated parameters from trapping in the local optimum, the parameters are recalculated considering the AoP error. The sensor parameters are defined as:

$$\mathbf{x} = \left[\, [\sigma_{I_i}]_{1\times 6} \;\; [\sigma_{d_i}]_{1\times 6} \;\; [\psi_i]_{1\times 6} \,\right]^T_{3\times 6} \tag{24}$$

The calculated residual vector of AoP and DoP obtained by parameter estimation can be expressed as:

$$\mathbf{R}(\mathbf{x}) = \begin{bmatrix} \phi(\mathbf{x}) - \phi_{w_n}(\mathbf{x}) \\ d(\mathbf{x}) - d_{w_n}(\mathbf{x}) \end{bmatrix} \tag{25}$$

where $\phi(\mathbf{x})$ and $d(\mathbf{x})$ represent the manually set AoP and DoP values, respectively; $\phi_{w_n}(\mathbf{x})$ and $d_{w_n}(\mathbf{x})$ represent the estimated AoP and DoP values, respectively. The parameters are estimated by minimising the square sum of the calculated residual of the AoP and the DoP with equal weights for each

https://doi.org/10.1017/S0373463321000308 Published online by Cambridge University Press

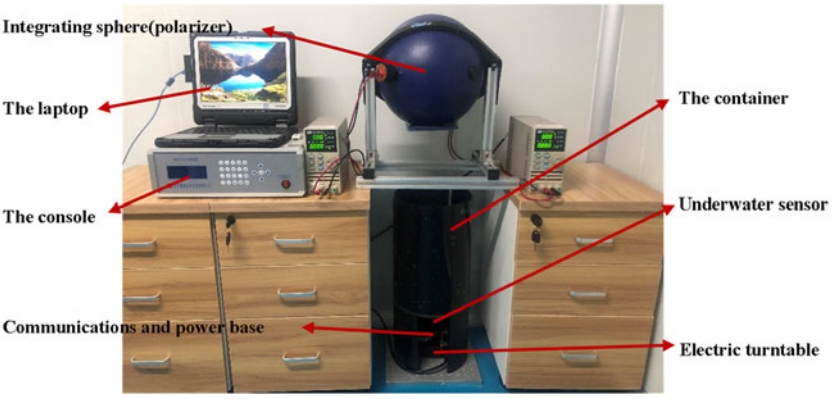

Figure 4. *Indoor calibration setup.*

measurement channel:

$$\mathbf{u} = \arg\min_{x}\left(\sum_{(i,j,k)} ||\mathbf{R}_{i,j,k}(\mathbf{x})||_2^2\right) \tag{26}$$

where (i, j, k) represents the combination of any three sensor channels. To solve the above optimisation problem, the initial value is determined by using Equation (24), and then the Secant Levenberg-Marquardt method is used for parameter iteration, the designed sensor parameters will be determined in the indoor calibration experiment.

6. Sensor performance experiments

This section presents the underwater experiments conducted to evaluate the sensor performance, including the indoor calibration experiment, indoor underwater experiment and outdoor underwater experiment.

6.1. Indoor calibration experiment

As the resolution values of AoP and DoP do not depend on the light intensity, the total light intensity is assumed to be an arbitrary constant. To avoid stray light interference, the experiment should be carried out under completely dark conditions. A light source with a stable output from an integrating sphere was used in the experiment, which was considered as an ideal light source.

The indoor calibration setup is shown in Figure 4, which includes an integrating sphere with polariser, a console, a laptop, an electric turntable, an underwater sensor and a communication and power base. The extinction ratio of the polariser is 9000:1, and the accuracy of the turntable is 0·01° per rotation. The polarisation sensor is fixed on the turntable and placed under the integrating sphere to align the centres of the integrating sphere, the sensor and the turntable. The light source output by the integrating sphere is processed by a linear polariser to obtain almost ideal polarised light with DoP of 1. The polarisation sensor collects one light intensity value every second with 1° rotation intervals of the turntable; 360 sets of figures can be collected for one whole rotation of the turntable.

To demonstrate the influence of the optical coupling coefficient involved in the underwater model, the following three cases are considered:

Case 1: The ideal model that only the installation angle of the polariser ψ is calibrated.

Case 2: The existing model that the light intensity coefficient σ_I and installation angle of the polariser ψ calibrated (σ_I and ψ) are calibrated.

https://doi.org/10.1017/S0373463321000308 Published online by Cambridge University Press

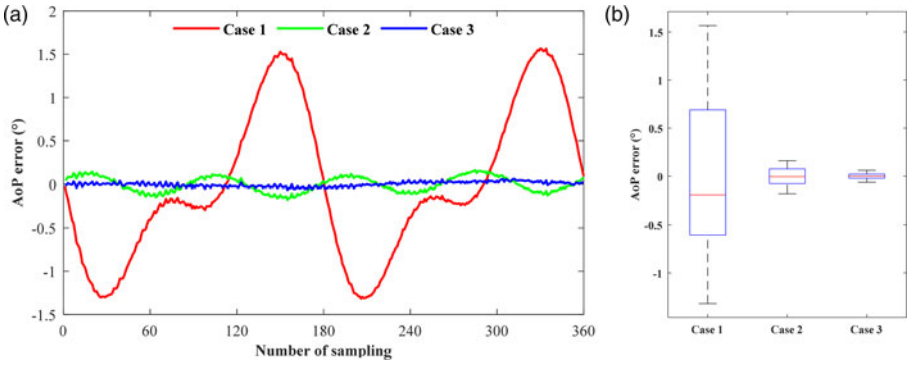

Figure 5. *AoP error curve and boxplot in three cases: (a) AoP error curve; (b) boxplot of AoP error.*

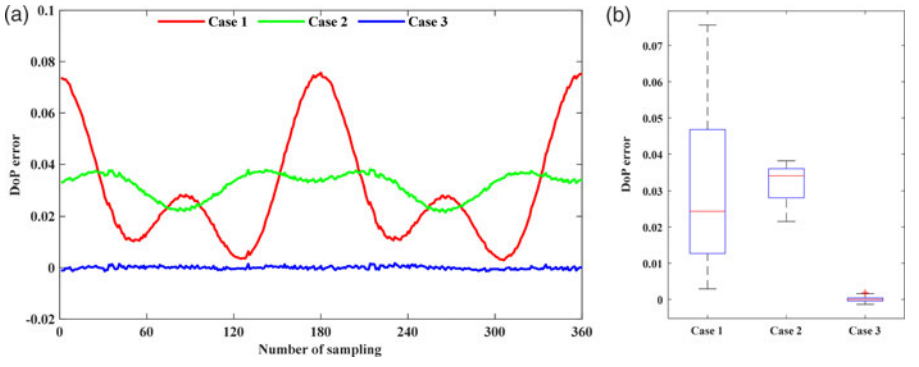

Figure 6. *DoP error curve and boxplot in three cases: (a) DoP error curve; (b) boxplot of DoP error.*

Case 3: The proposed underwater model that the light intensity coefficient σ_I, optical coupling coefficient σ_d and the installation angle of the polariser ψ are all calibrated.

The AoP results derived from all the three cases are illustrated in Figure 5. The red, green and blue lines represent the results of Case 1, Case 2 and Case 3, respectively.

For Case 1, the maximum AoP error is 1·5662°, and the standard deviation (SD) of the error is 0·8551°. Compared with Case 1, the AoP calculation accuracy of Case 2 is significantly improved with 0·1769° the maximum AoP error, and 0·0855° SD error. The maximum DoP errors of the two cases are 0·0757 and 0·0381 as shown in Figure 6. Compared with 0·0855° DoP error obtained by Case 1, the SD of DoP error is only 0·0049 with 77·82% improvement in Case 2. It is indicated that the existing model with the light intensity coefficient is more effective than the ideal model in calculating polarisation information.

It is apparent that the best accuracy is achieved by Case 3. Its error SD of AoP is 0·0266°, which is 68·89% lower than that of Case 2. The maximum and median errors are 0·0630° and 0·0006°, respectively. The DoP error SD obtained by Case 3 is only 0·0006 with 87·76% improvement in comparison with Case 2. The results show that the sensor accuracy is greatly improved when the optical coupling coefficient is introduced into the model of the underwater polarisation sensor. Therefore, the polarisation sensor model proposed in this paper has the potential to perform effectively underwater.

The obtained calibrated sensor parameters of each channel and normalised the light intensity coefficient are shown in Table 2.

6.2. Indoor underwater experiment

In this section, to validate the effectiveness of the antagonistic polarisation algorithm in different underwater environments, indoor underwater experiments considering the following cases

https://doi.org/10.1017/S0373463321000308 Published online by Cambridge University Press

Table 2. *Calibrated parameters of each channel.*

	Channel 1	Channel 2	Channel 3	Channel 4	Channel 5	Channel 6
σ_I	1·1340	1·1210	1·1938	1	1·1196	1·1341
σ_d	0·9574	0·9658	0·9613	0·9994	0·9652	0·9643
ψ	0	28·0648	56·9646	87·5411	116·8183	149·7196

were conducted:

1. Different light intensity: to test the effectiveness of the antagonistic polarisation algorithm at different light intensity.

   Case 1: increase the input light intensity
   Case 2: decrease the input light intensity

1. Different direction of incident light: to test the effectiveness of the antagonistic polarisation algorithm at different direction of incident light.

   Case 3: direct light
   Case 4: oblique light

1. Water surface fluctuates: to test the effectiveness of the antagonistic polarisation algorithm when the water surface is fluctuating.

   Case 5: Wavy water surface

The polarisation equipment is the same as that used in the indoor calibration experiment. The sensor was placed under the container to detect the light intensity. The polarised light produced by the integrating sphere passes through the water and is then captured by the polarisation sensor.

The comparison of performance in terms of AoP and DoP calculation accuracy between the independent polarisation algorithm and antagonistic polarisation algorithm is shown in Figure 7. It is shown that the AoP error is closer to zero by using the antagonistic polarisation algorithm. Table 3 lists the detailed AoP error comparison of the independent polarisation algorithm and antagonistic polarisation algorithm under the five different cases. It can be seen that the AoP accuracy achieved by the antagonistic polarisation algorithm is better than that of the independent polarisation algorithm under all five experimental cases. The mean values of AoP error are 0·0646°, 0·0616°, 0·0600°, 1·3445° and 0·1689°, respectively, for the independent polarisation algorithm, and 0·0610°, 0·0591°, 0·0566°, 0·8119° and 0·1399° for the antagonistic polarisation algorithm. In addition, the mean and SD of AoP errors are also lowered for the five cases with the antagonistic polarisation algorithm. Specifically, the mean of AoP error can be reduced by 39·61% and 55·01% reduction in SD of AoP error is achieved for Case 4.

From the DoP error comparison shown in Figure 7, it is obvious that the DoP error calculated based on the antagonistic polarisation algorithm is smoother and more stable than that of the independent polarisation algorithm. The detailed DoP error comparison results are shown in Table 4. It shows that the SD of DoP error of the antagonistic polarisation algorithm is smaller than that of the independent polarisation algorithm. The mean of the DoP error can be reduced by 60% and the highest percentage of improvement can reach up to 51·43% in SD of the DoP error. The mean DoP errors obtained by antagonistic polarisation algorithm are 0·0007, 0·0007, 0·0007, 0·0154 and 0·0013, which are smaller than those of the independent polarisation algorithm under all five circumstances.

The experimental results show that the AoP and DoP calculated with the antagonistic polarisation algorithm is more precise in different underwater scenarios. Apparently, the antagonistic polarisation algorithm is more robust against interference compared with the independent polarisation algorithm. It can be concluded that the antagonistic polarisation algorithm is more suitable in the low SNR underwater environment.

https://doi.org/10.1017/S0373463321000308 Published online by Cambridge University Press

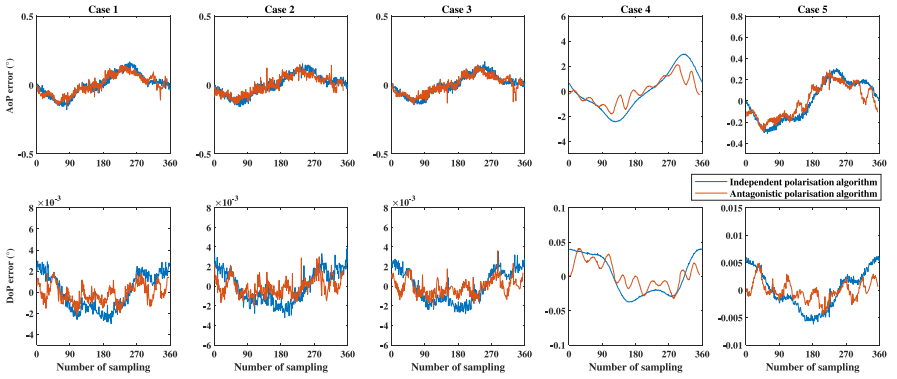

Figure 7. *Error curve of AoP and DoP in five cases: the first row is the AoP error curve in five cases and the second row is the DoP error curve in five cases; the orange line indicates the error calculated by the antagonistic polarisation algorithm and the blue line indicates the error calculated by the independent polarisation algorithm.*

Table 3. *Comparison of AoP error with independent polarisation algorithm and antagonistic polarisation algorithm.*

	Independent polarisation algorithm		Antagonistic polarisation algorithm		Percentage	
	Mean	SD	Mean	SD	Mean	SD
Case 1	0·0646°	0·0797°	0·0610°	0·0711°	5·57%	10·79%
Case 2	0·0616°	0·0746°	0·0591°	0·0682°	4·06%	8·95%
Case 3	0·0600°	0·0732°	0·0566°	0·0660°	5·67%	9·84%
Case 4	1·3445°	1·5805°	0·8119°	0·7110°	39·61%	55·01%
Case 5	0·1689°	0·1847°	0·1399°	0·1549°	17·17%	16·13%

Table 4. *Comparison of DoP error of independent polarisation algorithm and antagonistic polarisation algorithm.*

	Independent polarisation algorithm		Antagonistic polarisation algorithm		Percentage	
	Mean	SD	Mean	SD	Mean	SD
Case 1	0·0016	0·0017	0·0007	0·0009	60·00%	47·06%
Case 2	0·0015	0·0016	0·0007	0·0009	53·33%	43·75%
Case 3	0·0015	0·0016	0·0007	0·0008	53·33%	50·00%
Case 4	0·0267	0·0284	0·0154	0·0183	42·32%	35·56%
Case 5	0·0031	0·0035	0·0013	0·0017	58·06%	51·43%

6.3. Outdoor underwater experiment based on polarisation sensor

To evaluate the performance of the designed bionic polarisation sensor in terms of the polarisation measurement acquisition and the effectiveness for underwater heading determination, one static underwater test using the polarisation sensor combined with INS was conducted on 23 September 2019 in a clear swimming pool (40°20′N, 116°34′E) of 5·4 m × 2·8 m × 1·5 m. It was sunny with only a few clouds in the sky on that day. The outdoor experiment setup is shown in Figure 8. The algorithm to estimate the orientation with polarisation can be found in Yang et al. (2020).

https://doi.org/10.1017/S0373463321000308 Published online by Cambridge University Press

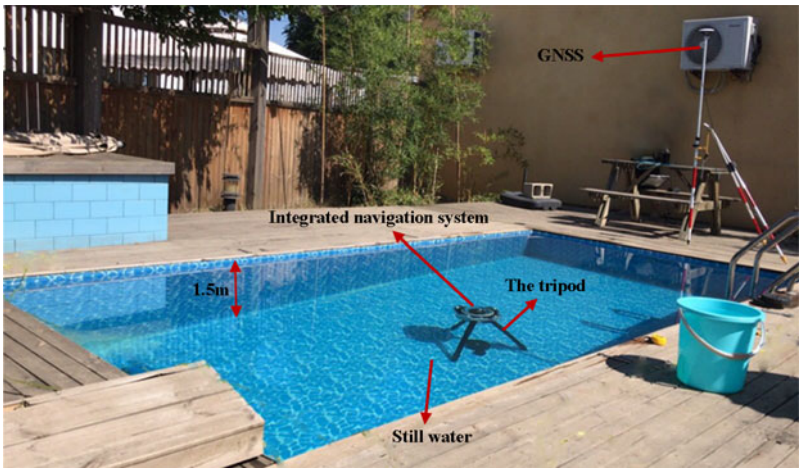

Figure 8. *Outdoor experiment setup.*

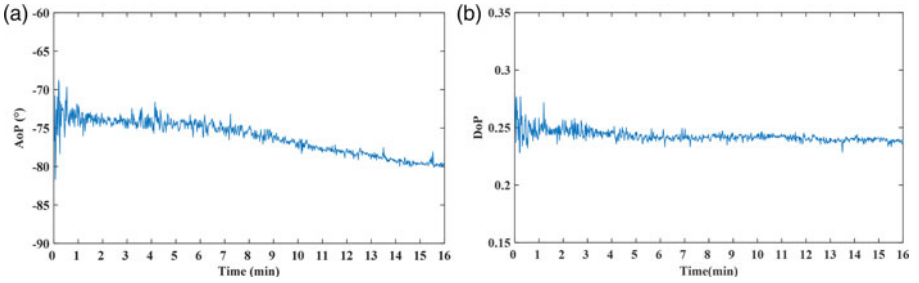

Figure 9. *Results of AoP and DoP underwater measurements: (a) AoP changes with the sun's position, (b) DoP maintains almost the same magnitude throughout the experiment.*

To provide the heading reference of the polarisation sensor, two UB280 GNSS receivers were set up and their antennas were placed on the same platform as the polarisation sensor with rough alignment. The antennas were then removed from the platform after acquiring the heading reference to prevent water damage. The heading reference was calculated based on differential GNSS (DGNSS) technique, which was 137·566° (positive direction: north by east) with an accuracy of 0·15°. The experiment lasted for 16 min, from 11:27 to 11:43 h. The angular drifts of the sun's azimuth and zenith during this period were 3·79° and 0·37°, respectively. The sensor was placed statically and horizontally in the pool at a depth of 0·6 m.

The calculated AoP and DoP measurements using the collected 16 min data are shown in Figure 9. Apparently, both AoP and DoP curves fluctuate sharply up and down at the beginning, and then are gradually converged. The AoP changes with the sun's position, which reflects the change of underwater polarisation pattern. The DoP maintains almost the same magnitude throughout the experiment. The higher fluctuations during the first 6 min can be attributed to the wavy water surface after placing the setup in the pool, which gradually became calm. The means of DoP error are respectively 0·2457 in the first 6 min and 0·2406 for the last 10 min. The SD of the calculated DoP measurements is 0·0074 for the first 6 min, and that is 0·0027 for the last 10 min. This indicates that the wavy water surface can affect the accuracy of the calculated AoP and DoP values. Nevertheless, the designed polarisation sensor can provide desired underwater polarisation information for practical applications.

The heading information obtained by the integration of the polarisation sensor compared with that derived from DGNSS is presented in Figure 10. The mean and SD of the estimated heading angle within the first 6 min are respectively 136·43° and 0·38°, and 136·73° and 0·51° for the last 10 min.

https://doi.org/10.1017/S0373463321000308 Published online by Cambridge University Press

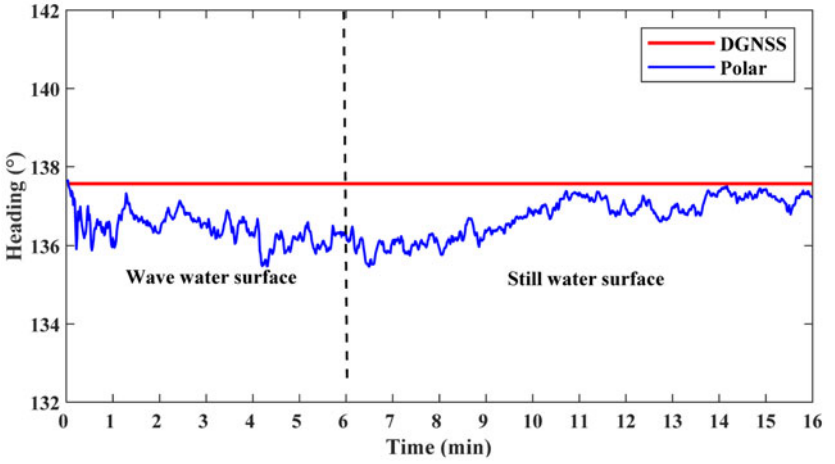

Figure 10. *The heading obtained by polarisation sensor: the red line indicates the heading calculated by the DGNSS and the blue line indicates the heading calculated by polarisation.*

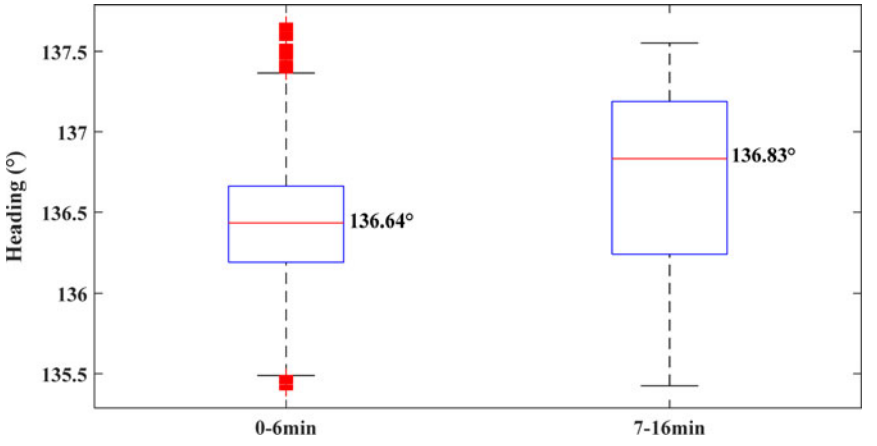

Figure 11. *Boxplot of the heading distributions.*

The distributions of the estimated heading angle values of the two periods with different water surface conditions are shown in Figure 11. The medians of heading are 136·64° and 136·83°, respectively. Due to the sensor error and individual operating error, there is an average constant error in calculated heading angle. This constant error will be studied and compensated for in the future.

These preliminary results suggest that an underwater polarisation pattern could be obtained by the designed underwater polarisation sensor at shallow depths, and the heading information can be determined by combining the polarisation sensor with INS. However, the uncertain interference underwater has a great influence on sensor performance. Due to the refraction of water, the polarised light will change with the change of the direction of incident light. Fluctuations of the water surface can also influence the underwater polarisation pattern. In the future, the disturbance of multiple optical effects will be seriously taken into consideration in sensor modelling to improve the performance of underwater bionic polarisation with real-time parameter calibration. In addition, the designed sensor has a narrow field of view that can only observe polarised light from limited directions. When the polarisation sensor is blocked, the sensor performance will greatly deteriorate underwater. In the future, to enhance the environmental adaptability, we will combine multiple sensors to capture polarised light underwater. All

https://doi.org/10.1017/S0373463321000308 Published online by Cambridge University Press

the above methods may contribute to improve the efficiency and accuracy of the underwater polarisation sensor.

7. Conclusion

In this paper, a bionic point-source underwater polarisation sensor with high spectral adaptability (400 nm–760 nm) is developed to acquire underwater polarised light. The model based on the underwater light intensity attenuation coefficient and optical coupling coefficient and an antagonistic polarisation algorithm are presented to achieve desirable polarisation performance in the low SNR environment underwater. The indoor underwater experiment shows that both AoP and DoP calculated with the antagonistic polarisation algorithm are more accurate than with the independent algorithm in underwater environments with different interferences. The outdoor underwater experiment proves that the designed bionic polarisation sensor can measure AoP and DoP for outdoor underwater environments and obtain heading information by combining with INS for the underwater vehicle in a static environment. It can be concluded that the designed polarisation sensor is promising for use in the stable and reliable determination of attitude for an AUV.

Acknowledgements. This work was supported by the National Natural Science Foundation of China (Grant number 62003017, Grant number 61627810, Grant number 61751302 and Grant number 61973012); Hangzhou Science and Technology Major Innovation Projects (Grant number 20182014B06).

References

Caruso, M. J. (2000). Applications of Magnetic Sensors for Low Cost Compass Systems. *IEEE 2000. Position Location and Navigation Symposium (Cat. No.00*CH*37062)*, San Diego, CA.

Chahl, J. and Mizutani, A. (2012). Biomimetic attitude and orientation sensors. *IEEE Sensors Journal*, **12**, 289–297.

Cheng, H. Y., Chu, J. K., Zhang, R., Tian, L. B. and Gui, X. Y. (2019). Underwater polarisation patterns considering single rayleigh scattering of water molecules. *International Journal of Remote Sensing*, **41**, 4947–4962.

Cronin, T. W. and Shashar, N. (2001). The linearly polarized light field in clear, tropical marine waters: Spatial and temporal variation of light intensity, degree of polarization and E-vector angle. *Journal of Experimental Biology*, **204**, 2461–2467.

Dupeyroux, J., Diperi, J., Boyron, M., Viollet, S. and Serres, J. (2017). A Novel Insect-Inspired Optical Compass Sensor for a Hexapod Walking Robot. *2017 IEEE/RSJ International Conference on Intelligent Robots and Systems (*IROS*)*, Vancouver, Canada.

Dupeyroux, J., Serres, J. R. and Viollet, S. (2019a). Antbot: A six-legged walking robot able to home like desert ants in outdoor environments. *Science Robotics*, **4**, eaau0307.

Dupeyroux, J., Viollet, S. and Serres, J. R. (2019b). An ant-inspired celestial compass applied to autonomous outdoor robot navigation. *Robotics and Autonomous Systems*, **117**, 40–56.

Emami, M. and Taban, M. R. (2018). A low complexity integrated navigation system for underwater vehicles. *The Journal of Navigation*, **71**, 1161–1177.

Fan, C., Hu, X. P., Lian, J. X., Zhang, L. L. and He, X. F. (2016). Design and calibration of a novel camera-based bio-inspired polarization navigation sensor. *IEEE Sensors Journal*, **16**, 3640–3648.

Giorgi, G., Teunissen, P. J. G., Verhagen, S. and Buist, P. J. (2010). Testing a new multivariate GNSS carrier phase attitude determination method for remote sensing platforms. *Advances in Space Research*, **46**, 118–129.

Heinze, S. and Homberg, U. (2007). Maplike representation of celestial E-vector orientations in the brain of an insect. *Science*, **315**, 995–997.

How, M. J., Porter, M. L., Radford, A. N., Feller, K. D., Temple, S. E., Caldwell, R. L., Marshall, N. J., Cronin, T. W. and Roberts, N. W. (2014). Out of the blue: The evolution of horizontally polarized signals in haptosquilla (Crustacea, Stomatopoda, Protosquillidae). *Journal of Experimental Biology*, **217**, 3425–3431.

Huang, Y., Wu, L. and Li, D. (2015). Theoretical research on full attitude determination using geomagnetic gradient tensor. *The Journal of Navigation*, **68**, 951–961.

Huang, Y. L., Zhang, Y. G. and Zhao, Y. X. (2019). Review of autonomous undersea vehicle navigation methods. *Journal of Unmanned Undersea Systems*, **27**, 232–253.

Kirk, J. T. O. (1983). *Light and Photosynthesis in Aquatic Ecosystems*. Cambridge: Cambridge University Press.

Kleinlogel, S. and Marshall, N. J. (2006). Electrophysiological evidence for linear polarization sensitivity in the compound eyes of the stomatopod crustacean *Gonodactylus chiragra*. *Journal of Experimental Biology*, **209**, 4262–4272.

Kleinlogel, S., Marshall, N. J., Horwood, J. M. and Land, M. F. (2003). Neuroarchitecture of the color and polarization vision system of the stomatopod haptosquilla. *Journal of Comparative Neurology*, **467**, 326–342.

Lambrinos, D., Kobayashi, H., Pfeifer, R., Maris, M., Labhart, T. and Wehner, R. (1997). An autonomous agent navigating with a polarized light compass. *Adaptive Behavior*, **6**, 131–161.

Lerner, A., Sabbah, S., Erlick, C. and Shashar, N. (2011). Navigation by light polarization in clear and turbid waters. *Philosophical Transactions of the Royal Society B-Biological Sciences*, **366**, 671–679.

Ma, T., Li, Y., Gong, Y. S., Wang, R. P., Sheng, M. W. and Zhang, Q. (2019). AUV bathymetric simultaneous localisation and mapping using graph method. *The Journal of Navigation*, **72**, 1602–1622.

Miller, P. A., Farrell, J. A., Zhao, Y. and Djapic, V. (2010). Autonomous underwater vehicle navigation. *IEEE Journal of Oceanic Engineering*, **35**, 663–678.

Müller, M. and Wehner, R. (1988). Path integration in desert ants, Cataglyphis fortis. *Proceedings of the National Academy of Sciences of the United*, **85**, 5287–5290.

Paull, L., Saeedi, S., Seto, M. and Li, H. (2014). AUV navigation and localization: A review. *IEEE Journal of Oceanic Engineering*, **39**, 131–149.

Powell, S. B., Garnett, R., Marshall, J., Risk, C. and Gruev, V. (2018). Bioinspired polarization vision enables underwater geolocalization. *Science Advances*, **4**, eaao6841.

Sabbah, S. and Shashar, N. (2007). Light polarization under water near sunrise. *Journal of the Optical Society of America A. Optics Image Science and Vision*, **24**, 2049–2056.

Sabbah, S., Barta, A., Gál, J., Horváth, G. and Shashar, N. (2006). Experimental and theoretical study of skylight polarization transmitted through Snell's window of a flat water surface. *Journal of the Optical Society of America A. Optics Image Science & Vision*, **23**, 1978–1988.

Stutters, L., Liu, H., Tiltman, C. and Brown, D. J. (2008). Navigation technologies for autonomous underwater vehicles. *IEEE Transactions on Systems, Man, and Cybernetics, Part C (Applications and Reviews)*, **38**, 581–589.

Thoen, H. H., How, M. J., Chiou, T. H. and Marshall, J. (2014). A different form of color vision in mantis shrimp. *Science*, **343**, 411–413.

Thoen, H. H., Chiou, T. H. and Marshall, N. J. (2017). Intracellular recordings of spectral sensitivities in stomatopods: A comparison across species. *Integrative and Comparative Biology*, **57**, 1117–1129.

Wang, Q. J., Li, Y. and Niu, X. J. (2016). Thermal calibration procedure and thermal characterisation of low-cost inertial measurement units. *The Journal of Navigation*, **69**, 373–390.

Wang, Y. J., Hu, X. P., Zhang, L. L. and He, X. F. (2017). Polarized light compass-aided visual-inertial navigation under foliage environment. *IEEE Sensors Journal*, **17**, 5646–5653.

Waterman, T. H. (1954). Polarization patterns in submarine illumination. *Science*, **120**, 927–932.

Waterman, T. H. (2006). Reviving a neglected celestial underwater polarization compass for aquatic animals. *Biological Reviews*, **81**, 111–115.

Wu, T., Tao, C. H., Zhang, J. H. and Liu, C. (2018). Correction of tri-axial magnetometer interference caused by an autonomous underwater vehicle near-bottom platform. *Ocean Engineering*, **160**, 68–77.

Xian, Z. W., Hu, X. P., Lian, J. X., Zhang, L. L., Cao, J. L., Wang, Y. J. and Ma, T. (2014). A novel angle computation and calibration algorithm of bio-inspired sky-light polarization navigation sensor. *Sensors*, **14**, 17068–17088.

Xian, Z. W., Hu, X. P. and Lian, J. X. (2015). Fusing stereo camera and low-cost inertial measurement unit for autonomous navigation in a tightly-coupled approach. *The Journal of Navigation*, **68**, 434–452.

Yang, J., Du, T., Liu, X., Niu, B. and Guo, L. (2019). Method and implementation of a bioinspired polarization-based attitude and heading reference system by integration of polarization compass and inertial sensors. *IEEE Transactions on Industrial Electronics*, **67**, 9802–9812.

Yang, J., Liu, X., Zhang, Q., Du, T. and Guo, L. (2020). Global autonomous positioning in GNSS-challenged environments: A bio-inspired strategy by polarization pattern. *IEEE Transactions on Industrial Electronics, Early Access*, doi:10.1109/TIE.2020.2994883

Zhou, G. H., Wang, J. W., Xu, W. J., Zhang, K. and Ma, Z. Q. (2017). Polarization patterns of transmitted celestial light under wavy water surfaces. *Remote Sensing*, **9**, 324.

Cite this article: Zhang T, Yang J, Guo L, Hu P, Liu X, Huang P, Wang C (2021). A bionic point-source polarisation sensor applied to underwater orientation. *The Journal of Navigation* **74**: 5, 1057–1072. https://doi.org/10.1017/S0373463321000308